# ALGINATE-BASED WOUND DRESSINGS EMBEDDED WITH MICROFLUIDIC-OBTAINED ZINC OXIDE NANOPARTICLES

Anca Elena ȚĂIN (ANASTASIU) [1], Alexandra Cătălina BÎRCĂ[1], Mihai Alexandru MINCULESCU[1], Alina Maria HOLBAN [2,3], Adelina-Gabriela NICULESCU[1,3], Alexandru Mihai GRUMEZESCU[1,3,*]

*This study presents the development of alginate-based wound dressings embedded with ZnO nanoparticles synthesized via a microfluidic approach using a cross-shaped chip. Two nanoparticle samples were prepared and characterized by XRD, SEM, and DLS to optimize properties toward antimicrobial applications. Three types of dressings were fabricated: alginate alone, alginate with ZnO nanoparticles, and alginate with both ZnO nanoparticles and Mimosa powder. Comprehensive analyses (FTIR, SEM, swelling, degradation, antimicrobial assays) demonstrated that microfluidic parameters influence nanoparticle properties and that ZnO- and Mimosa-enriched dressings exhibit enhanced antimicrobial activity and physicochemical properties suitable for promoting wound healing.*

**Keywords**: ZnO nanoparticles, alginate hydrogels, advanced wound dressings, antimicrobial activity, wound healing

## 1. Introduction

The skin, as the body's first line of defense, is prone to various open injuries that can be readily colonized by bacteria [1]. Wound infections pose a significant healthcare challenge due to biofilm formation, the increasing prevalence of antibiotic-resistant bacterial strains, and the adverse consequences on healing dynamics, especially in chronic wounds [1-3]. The presence of pathogenic microorganisms in the wound bed has been linked to persistent inflammation, tissue damage, delayed healing, defective wound closure, and even systemic complications if not addressed in a timely and efficient manner [1,3-7].

The standard approach for managing cutaneous wounds involves applying various dressings that provide protection and absorb wound exudate. In clinical practice, conventional wound dressings, such as gauze, cotton wool, lint, and basic bandages, are widely used due to their accessibility and simplicity [8,9]. However,

[1] Department of Science and Engineering of Oxide Materials and Nanomaterials, National University of Science and Technology POLITEHNICA Bucharest, Romania; e-mails: anca_tain@yahoo.com; ada_birca@yahoo.com; mihaiminculescu27@yahoo.com, adelina.niculescu@upb.ro; agrumezescu@upb.ro.
[2] Faculty of Biology, University of Bucharest, Romania; e-mail: alina_m_h@yahoo.com
[3] Research Institute of the University of Bucharest—ICUB, University of Bucharest, Romania
* Corresponding author: Alexandru Grumezescu, e-mail: agrumezescu@upb.ro

they act mainly as passive barriers, offering limited fluid absorption, lacking intrinsic antimicrobial properties, and failing to maintain the moist environment essential for tissue regeneration, which is especially problematic in infected, chronic, or necrotic wounds [9-11]. Thus, there is a growing need for advanced wound dressings that combine protective, absorptive, and bioactive functions to support faster and more effective healing [12-15].

In this context, hydrogels have emerged as a superior alternative, providing improved healing outcomes. Unlike passive traditional materials, hydrogels maintain a moist wound interface, promote cell proliferation, and allow for the incorporation of bioactive agents, offering multifunctional performance in wound care [11]. Among them, alginate-based hydrogels are particularly promising owing to their natural origin, biocompatibility, and ability to rapidly gel upon contact with divalent or trivalent cations [16]. Alginate dressings effectively absorb exudates, form in situ hydrogels, and support re-epithelialization while reducing bacterial load [10,17-19]. Furthermore, alginate's muco-adhesiveness and tunable porosity make it an excellent carrier for drugs and nanoparticles [20]. Still, native alginate hydrogels suffer from limited mechanical strength and poor cell adhesion, which are crucial for applications in skin regeneration. To address these limitations, the incorporation of inorganic nanomaterials into the alginate matrix has been proposed as a strategy to enhance its mechanical integrity and biofunctionality [20].

Zinc oxide nanoparticles (ZnO NPs) are particularly suitable additives, known for their strong antimicrobial activity and relatively low cytotoxicity compared to other metal-based nanomaterials such as silver or copper [21,22]. ZnO NPs exert their antibacterial activity by disrupting bacterial membranes, inducing oxidative stress, and interfering with essential metabolic pathways [21]. Their incorporation into alginate-based hydrogels enhances both the mechanical integrity and antimicrobial efficacy of the composite dressing, which are crucial factors in managing infected or chronic wounds [20,23-26]. This aligns well with the current push toward safer, multifunctional materials for advanced wound care [10].

The properties of nanomaterials are closely correlated with their synthesis method, which, in the case of ZnO NPs, can vary from conventional batch synthesis methods employed for decades to more modern and reliable techniques [27]. In particular, microfluidic synthesis offers a highly controlled and efficient method for producing ZnO NPs with superior physicochemical properties compared to traditional synthesis options. By enabling precise regulation of reaction conditions and environmentally friendly production, microfluidic platforms yield ZnO NPs with uniform size, high crystallinity, and improved dispersibility and stability, which are critical aspects for biomedical applications, such as advanced wound dressings [22,27,28].

In addition to nanomaterials, herbal agents have been used in traditional medicine for a long time to promote wound healing [29]. Among these, *Mimosa*

*pudica* has a rich phytochemical profile, including alkaloids, tannins, amino acids, and fatty acids like linoleic and oleic acid, which contribute to its anti-inflammatory, antimicrobial, and tissue-regenerative effects [30]. Studies have shown that Mimosa bark powder incorporated into hydrogels can reduce wound area, accelerate re-epithelialization, and stimulate fibroblast activity, making it a promising adjunct in modern wound dressings [29,31]. Its high tannin content likely contributes to its wound-healing efficacy through astringent action, supporting its utility for skin lesions and promoting hemostasis [32]. Thus, integrating Mimosa powder into hydrogels represents a natural and bioactive strategy to enhance the regenerative potential of advanced wound care materials.

Despite their individual appealing properties, there is a current research gap concerning the synergistic combination of alginate, microfluidically synthesized ZnO, and Mimosa in a dressing format. In this respect, this study aims to develop and evaluate alginate-based wound dressings incorporating ZnO NPs synthesized via microfluidics and supplemented with Mimosa powder to enhance antimicrobial and regenerative properties.

## 2. Materials and Methods

### *2.1. Materials*

For fabricating the wound dressings, the following reagents were employed: sodium alginate ($NaC_6H_7O_6$), zinc nitrate hexahydrate ($Zn(NO_3)_2 \cdot 6H_2O$), sodium hydroxide (NaOH), and methanol ($CH_3OH$). Ultrapure water was utilized for all experiments.

### *2.2. ZnO nanoparticles synthesis*

ZnO NPs were produced within a cross-shaped microfluidic platform, having the experimental design described in our previous studies [33,34]. Two solutions were simultaneously introduced into the microfluidic channels via a four-channel peristaltic pump, connected to three inlet hoses. Solution 1 (S1), serving as the zinc precursor, consisted of a 5% w/v solution of zinc nitrate hexahydrate in methanol and was introduced into the synthesis chip via the central port. Solution 2 (S2), a 2% w/v sodium hydroxide solution prepared in ultrapure water, was delivered through two separate side ports. The solutions reacted at the intersection of the microfluidic channels, leading to zinc hydroxide precipitation.

To produce ZnO NPs, the resulting product was processed with Synthwave equipment. The processing parameters were 160°C temperature, 10 bar load pressure, and 20 minutes processing time. The resulting samples were washed three times with ultrapure water by centrifugation. Following this, the product was dried in an oven at 60°C for 8 hours. Finally, the product was grinded into a fine powder. Two distinct samples were prepared with different operating conditions: Sample 1

- S1 flow of 15 rotations per minute (RPM) and S2 at 30 RPM, and Sample 2, S1 - 30 RPM, and S2 - 15 RPM.

### *2.3. Hydrogel synthesis*

Following the physicochemical characterization of the two zinc oxide samples synthesized via microfluidic methods, the ZnO_30-15 sample was selected, based on analytical results, for incorporation into dressings intended for chronic wound therapy. Sodium alginate, used as the hydrogel matrix, was prepared as a 5% w/v stock solution. To obtain the final material of interest and evaluate the contribution of each component, three hydrogels were formulated. The first hydrogel, serving as a control, consisted solely of the viscous alginate solution and was named ALG. The second hydrogel, referred to as Alg_ZnO_30-15, contained ZnO NPs (ZnO_30-15) incorporated into the alginate matrix at a concentration of 2.5 mg/mL, relative to the total mass of the dressing. The third hydrogel included a natural component with potential regenerative effects, namely Mimosa powder, introduced at the same concentration as the zinc oxide nanoparticles to achieve a 1:1 ratio between antimicrobial and regenerative activity. The hydrogels were left in the freezer for 12 hours and then subjected to lyophilization. Table 1 summarizes sample codification for better clarity in understanding further discussed results.

*Table 1*

**Sample codification**

| Name | Code |
|---|---|
| First sample of ZnO nanoparticles | ZnO_15-30 |
| Second sample of ZnO nanoparticles | ZnO_30-15 |
| Control hydrogel | Alg |
| ZnO hydrogel | Alg_ZnO_30-15 |
| ZnO Mimosa hydrogel | Alg_ZnO_30-15_Mimosa |

### *2.4. Characterization methods*

ZnO NP crystallinity evaluation was performed via X-ray diffraction, using a PANalytical Empyrean model diffractometer purchased from PANalytical, Almelo, The Netherlands. Grazing Incidence X-ray Diffraction (GIXRD) measurements were performed at room temperature, with an angle of incidence $\omega = 0.5°$ for Bragg angle values of $2\theta$ between 10° and 80°, using Cu Kα radiation with $\lambda = 1.5406$ Å (40 mA and 45 kV).

For morphological investigations, SEM analysis was performed on both nanoparticles and alginate-based hydrogels. The samples were fixed on a carbon-bearing slide and placed in an Inspect F50 scanning electron microscope analysis chamber purchased from Thermo Fisher - FEI (Eindhoven, The Netherlands). The micrographs were obtained by recording the resulting secondary electron beam and electron beam scattering with an energy of 30 keV.

DLS measurements were performed using a DelsaMax Pro-type device equipped with a 532 nm laser. The powders were dispersed in ultrapure water at room temperature. Using an ultrasonic bath, all samples were subjected to ultrasound for 10 minutes to achieve the best possible dispersion. For the identification of functional groups, FTIR analysis was performed on all dressing samples. Using a ZnSe crystal of a Thermo iN10-MX FTIR spectrometer purchased from Thermo Fisher Scientific, Waltham, USA, spectra were collected within the 4000 – 400 $cm^{-1}$ wavenumber interval.

The lyophilized hydrogels were cut into cylindrical shapes with a diameter of 5 mm to evaluate the swelling capacity of the obtained materials. Each sample was immersed in phosphate buffer solution (PBS), and the swelling rate was determined using the formula from Eq. (1)

$$\text{Swelling ratio} = \frac{Wt - Wi}{Wi}\ x\ 100\% \quad (1)$$

where Wi is the initial mass of the sample (before PBS immersion), and Wt is the time point mass after immersion and weighted at different times.

To assess biofilm formation, materials were cut into circular 5 mm pieces and sterilized under UV light for 20 min per side. Each piece was placed in a well of a sterile 96-well plate, followed by 2 mL of liquid medium (plain broth) and 10 µL of 0.5 McFarland microbial suspension. Plates were incubated at 37°C for 24 h, then washed with AFS and refreshed with new medium for an additional 24 h incubation. The materials were then washed, transferred to sterile tubes with 1 mL of AFS, and vortexed for 30 s to detach the biofilm cells. The resulting suspension was diluted and plated to quantify CFU/mL. The dressings' antibacterial activity was evaluated using a modified disc diffusion method, following the 2021 CLSI guidelines. Bacterial inocula (0.5 McFarland, ~$1.5 \times 10^8$ CFU/mL) were prepared from 18–24 h cultures and uniformly spread on nutrient agar plates (pH 7.2–7.4, 4 mm thick). Hydrogel discs were aseptically placed on the inoculated agar and incubated (37 °C, 24 h). Inhibition zone diameters were measured as indicators of antibacterial efficacy.

## 3. Results and Discussion

XRD analysis of the two NP powders (Fig. 1) revealed a single phase in the samples, which is zinc oxide. Both examined materials displayed high crystallinity, with prominent peaks identified for diffraction planes (100), (002), (101), (102), (110), (103), (200), (112), (201), (004), and (202) – which are characteristic to ZnO hexagonal (wurtzite) structure with preferred orientation along (101) plane [35-37]. The ZnO_15-30 sample exhibits an enhanced intensity due to an excess use of sodium hydroxide solution during the synthesis process, which was facilitated by the rotational speed employed.

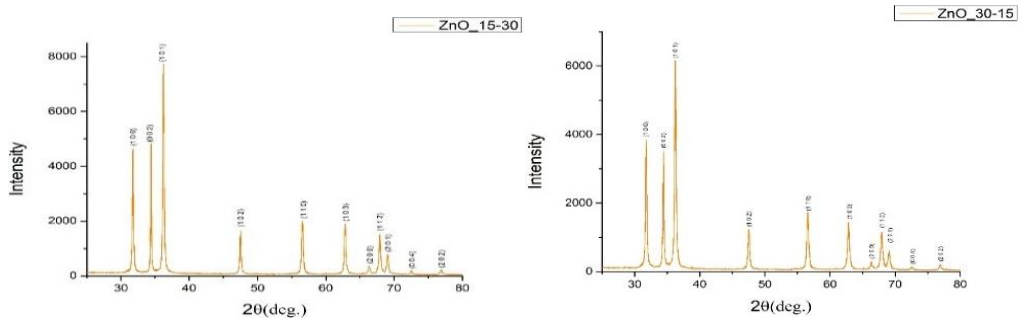


Fig.1. The diffractogram of ZnO_15-30 and ZnO_30-15.

Also, the average crystallite size was calculated using the Debye-Scherrer formula from Eq. (2).

$$D = \frac{K * \lambda}{\beta * \cos\theta} \tag{2}$$

By the calculation for sample ZnO_15-30, the average crystallite size corresponds to a value of 29.13 nm, and the value for sample ZnO_30-15 is 31.67 nm. The slightly larger crystallite size observed in ZnO_30-15 suggests that the different flow rate ratios used during microfluidic synthesis influenced the nucleation and growth processes of ZnO NPs. The morphological and dimensional characteristics of NPs have been determined through SEM analysis. The micrographs obtained at 100,000x and 200,000x magnifications are included in Fig.2.

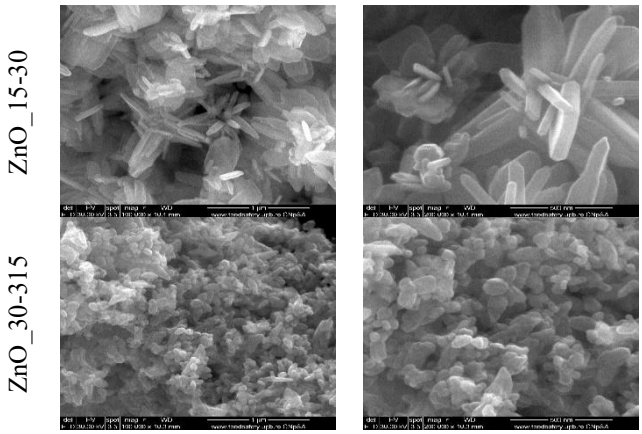


Fig.2. SEM images for ZnO_15-30 and ZnO_30-15.

Although essentially the same material is examined, different morphologies can be observed due to the parameters chosen for the synthesis. As a result of an excessive amount of sodium hydroxide entering the reaction at the microfluidic platform, the ZnO_15-30 sample exhibits morphology in the form of rods, gathered

in the shape of flower-like ZnO clusters. Differently, for the ZnO_30-15 sample, quasi-spherical morphologies were identified, with a slight elongation tendency.

The micrographs obtained have also enabled the generation of particle size distributions and the calculation of the average particle size for each sample (Fig. 3). The ZnO_15-30 sample is found in the size range of 153.19 nm and 497.8 nm with an average size of 302.47±13.74 nm, whereas the ZnO_30-15 sample is found between 40.69 nm and 121.72 nm with an average size of 73.34±3.42 nm.

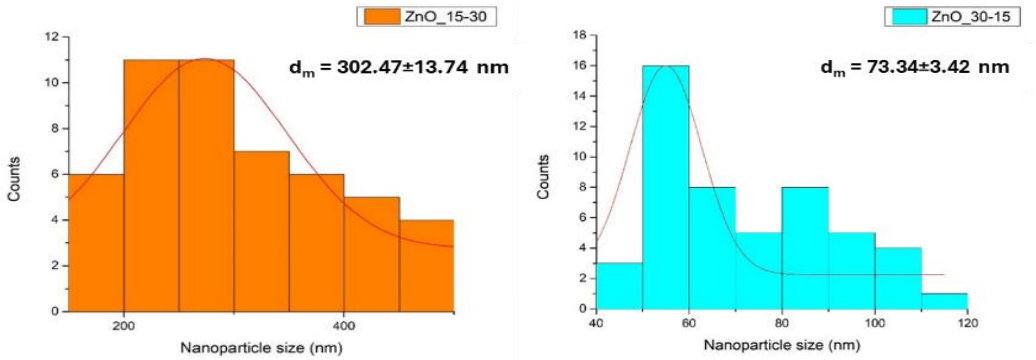


Fig.3. Particle size distribution for ZnO_15-30 and ZnO_30-15.

DLS analysis (Fig.4) was performed to obtain information regarding the Zeta potential and size distribution profile of particles in suspension.

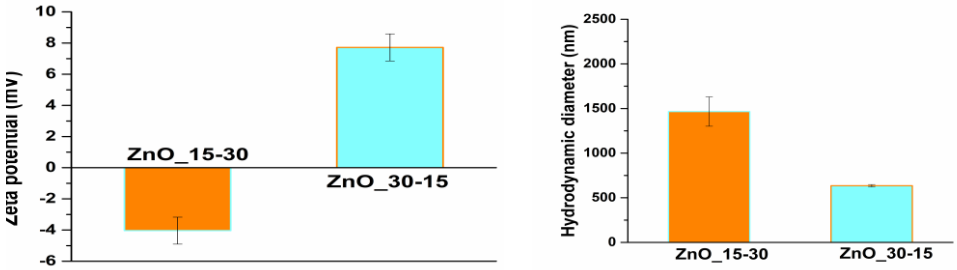


Fig.4. Zeta Potential (mV) and hydrodynamic diameters (nm) for the ZnO_15-30 and ZnO_30-15 samples.

Notably, the zeta potential of the ZnO_30-15 sample exhibited a nearly double absolute value compared to the ZnO_15-30 sample, suggesting that the ZnO_30-15 sample displays moderate stability in solution, whereas the ZnO_15-30 sample displays unfavorable values with relatively unstable behavior. A strong correlation is observed between the hydrodynamic diameter and the physical particle size. The flower-like ZnO rods in the ZnO_15-30 sample are characterized by larger hydrodynamic diameter values, specifically 1465.63 nm. In contrast, the ZnO_30-15 sample exhibits a smaller hydrodynamic diameter value of 635.56 nm, consistent with the observations from SEM micrographs. Based on their more

suitable physico-chemical properties, ZnO_30-15 NPs were chosen for further incorporation into the hydrogel.

Following the detailed physicochemical characterization of the synthesized ZnO NPs, further analyses were conducted to evaluate their incorporation into hydrogel matrices and to assess the properties of the resulting functionalized hydrogels.

FT-IR spectra were recorded for all hydrogel samples, as comparatively displayed in Fig. 5. The FT-IR spectra of all three hydrogel dressings exhibit characteristic bands attributable to the alginate matrix, confirming its structural role in all formulations. A broad absorption band centered around 3200 $cm^{-1}$ corresponds to O–H stretching vibrations, indicating the hydrophilic nature of alginate [38,39]. Additional prominent peaks observed near 2934 $cm^{-1}$ (C–H stretching), 1593 $cm^{-1}$ (asymmetric $COO^-$ stretching), 1409 $cm^{-1}$ (symmetric $COO^-$ stretching), and 1027 $cm^{-1}$ (C–O–C stretching) are consistent with alginate's functional groups [34,40]. Notably, the spectra of the Alg_ZnO_30-15 and Alg_ZnO_30-15_Mimosa samples exhibit an additional band near 400 $cm^{-1}$, attributed to Zn–O stretching, confirming the successful incorporation of ZnO NPs. In addition to the identification of characteristic functional groups, subtle shifts in the carboxylate and hydroxyl stretching bands, along with changes in their intensities, suggest strong interactions between ZnO NPs, Mimosa components, and the alginate matrix, supporting the effective incorporation and molecular-level integration of bioactive agents within the hydrogel network.

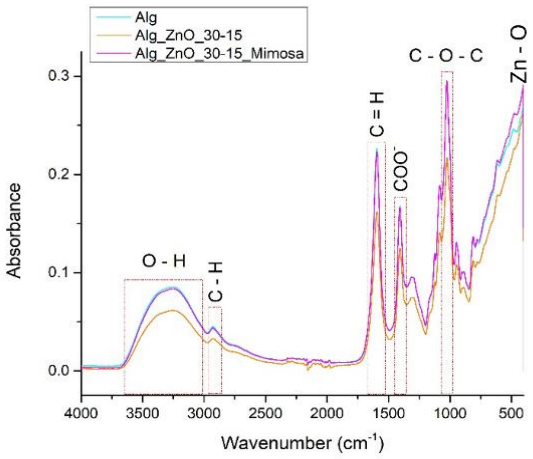


Fig.5. FTIR spectra recorded for Alg, Alg_ZnO_30-15, and Alg_ZnO_30-15_Mimosa samples.

Furthermore, the hydrogel-based materials were characterized using SEM to enable visualization of their morphology and microstructure (Fig.6). The three hydrogel samples exhibit a porous structure, which is desirable in wound dressing applications, as this type of architecture fosters cell adhesion and accelerates the

healing process by allowing the passage of fluids and immune cells [41,42]. Moreover, Alg_ZnO_30-15 and Alg_ZnO_30-15_Mimosa hydrogels display a homogeneous distribution of ZnO nanoparticles within the alginate polymer matrix. The NPs are present on the surface of the matrix as well as embedded in its thin walls, ensuring optimal dispersion and functionality. The EDS analysis (Fig.7) confirms the presence of elements characteristic of the alginate matrix, specifically carbon, oxygen, and sodium. Additionally, the successful incorporation of zinc oxide into the two functionalized hydrogels (Alg_ZnO_30-15 and Alg_ZnO_30-15_Mimosa) is demonstrated by the clear detection of zinc.

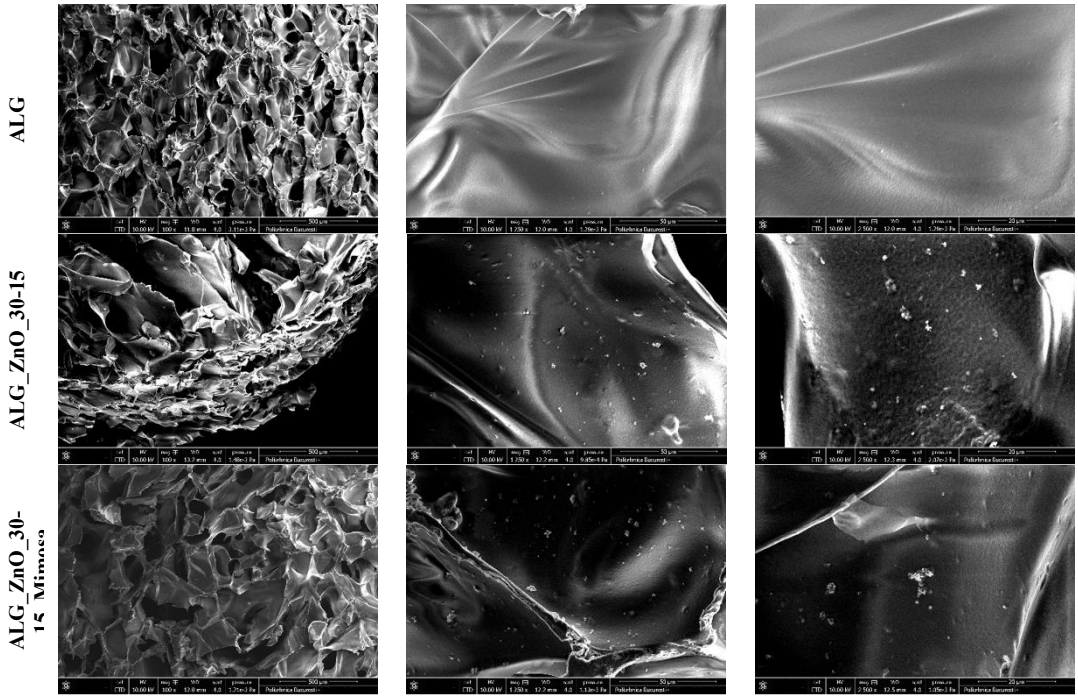


Fig.6. SEM images for Alg, Alg_ZnO_30-15, and Alg_ZnO_30-15_Mimosa.

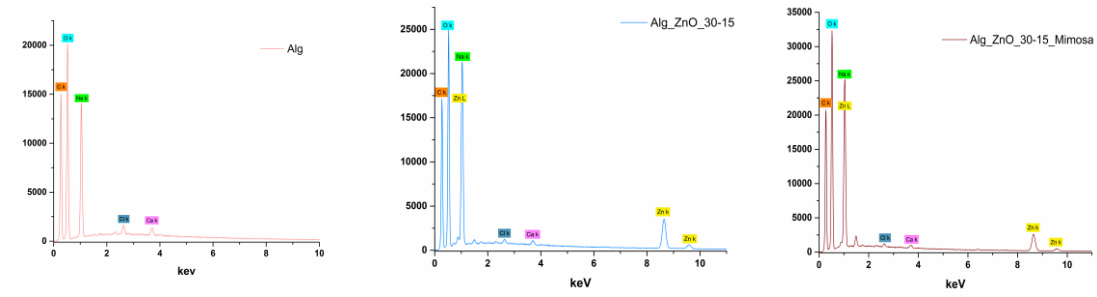


Fig.7. EDS results for Alg, Alg_ZnO_30-15, and Alg_ZnO_30-15_Mimosa.

SEM investigations have also allowed determination of pore size distribution (Fig.8). The Alg control sample has a pore size range between 40.53 µm and 167.5 µm, with an average size of 98.89±6.21 µm; the Alg_ZnO_30-15 sample has pores ranging between 60.91 µm and 224.69 µm, with an average size of 125.57±6.97 µm, while the Alg_ZnO_30-15_Mimosa sample exhibited pores ranging between 65.28 µm and 187 µm with an average size of 110.33±4.14 µm. The pore size differences observed in SEM might be attributed to interactions between alginate and additives, which can influence the crosslinking density and internal architecture of the hydrogels. ZnO, for example, may act as a mild crosslinking agent, slightly loosening the polymer network and increasing pore size [43] (as seen in Alg_ZnO_30-15).

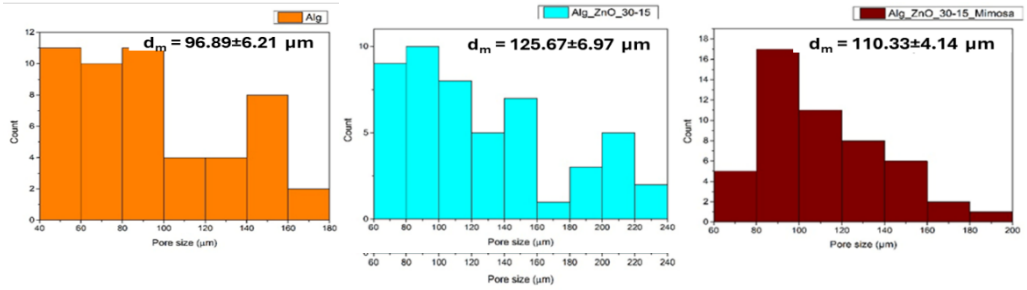


Fig.8. Pore size distribution histogram for: Alg, Alg_ZnO_30-15, Alg_ZnO_30-15_Mimosa.

Given their intended application as wound dressings, the hydrogels were also evaluated from the perspective of their swelling rate (Fig. 9). The initial measurement, taken 15 minutes after application, revealed that all dressings exhibited a swelling rate exceeding 100%. The Alg sample displayed the highest absorption capacity at 274%, while the Alg_ZnO_30-15 and Alg_ZnO_30-15_Mimosa samples showed rates of 151% and 131%, respectively. The decrease in absorption capacity compared to the Alg control sample can be attributed to the presence of ZnO NPs and Mimosa powder in the alginate polymer structure. During the evaluation period, all three hydrogels maintained swelling rates above 100% until 240 minutes. After the first 4 hours, a gradual decline in the swelling rate was observed, which may be attributed to the hydrogel network reaching structural saturation, followed by partial relaxation or erosion of the polymer matrix and ion exchange with the PBS medium, collectively reducing its fluid retention capacity. Although the addition of ZnO NPs and Mimosa powder to the alginate gel resulted in lower swelling rates compared to the control sample, the dressings' ability to retain liquids was still satisfactory, making them suitable for their intended application.

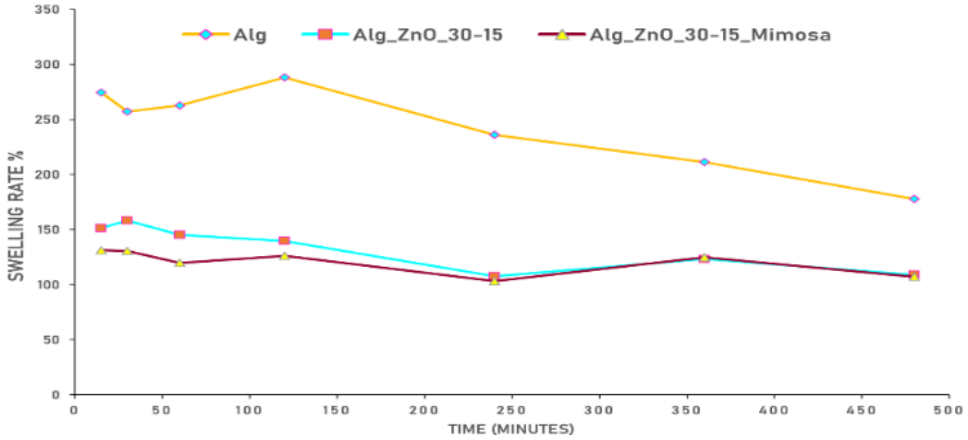


Fig.9. Swelling rate evaluation of Alg, Alg_ZnO_30-15, Alg_ZnO_30-15_Mimosa in PBS.

To evaluate the antimicrobial efficacy of the developed hydrogels, their activity was assessed against both Gram-positive (*Staphylococcus aureus*) and Gram-negative (*Escherichia coli*) bacterial strains. The evaluation focused specifically on the inhibition of biofilm formation, which was quantitatively measured after 24 hours of incubation (Fig.10). This approach allowed for the assessment of the hydrogels ability to prevent bacterial adhesion and early biofilm development, key factors in the treatment of chronic wounds where biofilm-related infections are a major concern. The results revealed significant differences among the three tested formulations. The control hydrogel (ALG), composed solely of alginate, exhibited the highest CFU values, indicating extensive bacterial proliferation and mature biofilm formation. In contrast, the hydrogel incorporating zinc oxide nanoparticles (ALG_ZnO_30-15) demonstrated a reduction in CFU, confirming the antimicrobial efficacy of ZnO in limiting bacterial adhesion and early biofilm development. Notably, the hydrogel containing both ZnO nanoparticles and Mimosa powder (ALG_ZnO_30-15_Mimosa) showed the lowest CFU counts, suggesting a synergistic effect between the inorganic antimicrobial agent and the natural bioactive compound. This dual action likely contributes not only to bacterial inhibition but also to enhanced wound healing potential. Overall, these findings support the superior anti-biofilm performance of the ZnO- and Mimosa-loaded hydrogel, making it a promising candidate for use in chronic wound dressings where biofilm control is essential. Nonetheless, this component was added to the hydrogel composition to improve its skin regeneration capabilities [32,44], yet its effect remains to be determined in future *in vitro* and *in vivo* studies.

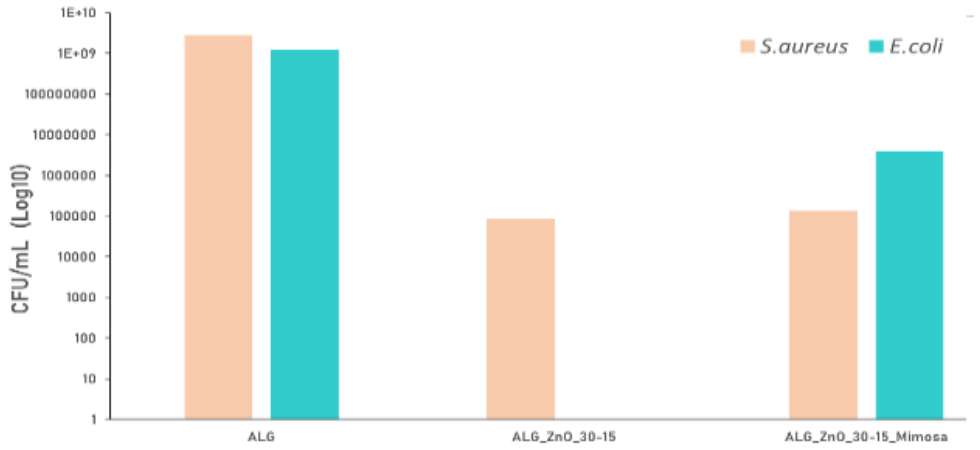


Fig.10. Graphical representation of the biofilm inhibition of Alg, Alg_ZnO_30-15, Alg_ZnO_30-15_Mimosa dressings after 24 hours of incubation with *S.aureus* and *E.coli*.

Regarding the inhibition zone diameters, the results are presented in Fig. 11.

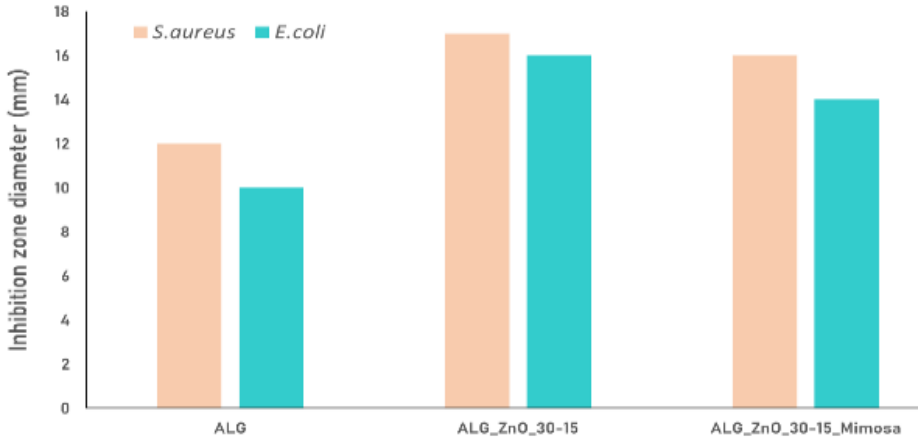


Fig.11. Inhibition zone diameter (mm) of Alg, Alg_ZnO_30-15, Alg_ZnO_30-15_Mimosa.

The results clearly demonstrated the antimicrobial efficacy of the functionalized hydrogels, as evidenced by the increased diameter of the inhibition zone compared to the control sample. In contrast, the hydrogel containing zinc oxide nanoparticles (ALG_ZnO_30-15) produced a larger inhibition zone, indicating effective diffusion of ZnO into the culture medium and pronounced bactericidal activity. The mechanism of action of ZnO is well-documented and includes the release of $Zn^{2+}$ ions, the generation of reactive oxygen species (ROS), and the disruption of bacterial membrane integrity. A remarkable effect was observed, as well, in the hydrogel formulated with both ZnO and Mimosa powder (ALG_ZnO_30-15_Mimosa). This result suggests a synergistic interaction between ZnO and the bioactive compounds present in *Mimosa pudica*. Therefore, these

findings support the potential of ZnO- and Mimosa-based formulations as advanced antimicrobial delivery systems for chronic wound treatment, where the inhibition of bacterial colonization and biofilm formation is critical to therapeutic success.

Overall, the comprehensive characterization of the developed hydrogels confirmed the successful integration of ZnO nanoparticles and Mimosa powder into the alginate matrix. Microfluidic synthesis parameters significantly influenced nanoparticle morphology, size, crystallinity, and stability—factors that directly impacted the hydrogel's porosity, swelling behavior, and antimicrobial activity. SEM analysis revealed well-distributed pores and nanoparticles, while the FTIR spectra supported the chemical compatibility between the components. The enhanced antimicrobial performance of ZnO and Mimosa-enriched hydrogels, particularly against *S. aureus* and *E. coli*, highlights their therapeutic potential. Together, these results demonstrate a synergistic effect between structural, physicochemical, and biological properties, supporting the hydrogel's application as a multifunctional wound dressing.

## 4. Conclusions

Wound infections remain a significant clinical challenge due to the increasing prevalence of antibiotic-resistant bacterial strains. This study investigated the development of alginate-based dressings functionalized with ZnO nanoparticles, synthesized via microfluidic technology and hydrothermal method, which offers precise control over nanoparticle characteristics. When dealing with nanoparticles intended for biomedical applications, their physicochemical properties are closely interlinked with their biological performance. Therefore, in the present study we employed a combined synthesis approach to obtain zinc oxide nanoparticles. The first step, based on a microfluidic method, enabled the rapid and homogeneous mixing of reactants within the microchip, which in turn promoted controlled nucleation and the formation of nanoparticles with small and uniform sizes. Since the as-obtained phase corresponded to zinc hydroxide, a subsequent hydrothermal treatment was applied to convert this intermediate into crystalline zinc oxide, while simultaneously allowing fine-tuning of particle morphology and size through synthesis parameters such as temperature and pressure. This hybrid approach leverages the precision of microfluidics and the versatility of the hydrothermal method, ultimately yielding ZnO nanoparticles with well-controlled dimensions and morphologies. The microfluidic approach enabled the production of two ZnO samples (ZnO_15-30 and ZnO_30-15), with ZnO_30-15 demonstrating superior properties for biomedical applications. Three hydrogel formulations were developed: alginate alone (Alg), alginate with ZnO nanoparticles (Alg_ZnO_30-15), and alginate with both ZnO and Mimosa powder (Alg_ZnO_30-15_Mimosa). SEM analysis confirmed the porous structure and uniform nanoparticle distribution

within the alginate matrix, unaffected by the addition of ZnO nanoparticles or/and Mimosa powder. The resulting composite dressings exhibited favorable physicochemical properties and antimicrobial activity, highlighting the benefits of microfluidic synthesis over conventional methods. This strategy offers a promising and scalable solution for enhancing wound healing and preventing infections, particularly in cases complicated by microbial colonization. The findings support further *in vitro* and *in vivo* studies to validate the safety, efficacy, and therapeutic potential of these nanocomposite hydrogels in clinical wound management.

## REFERENCES

1. Sen, C.K. Human Wounds and Its Burden: An Updated Compendium of Estimates. Advances in Wound Care **2019**, 8, 39-48, doi:10.1089/wound.2019.0946.
2. Falcone, M.; et al. Challenges in the management of chronic wound infections. Journal of Global Antimicrobial Resistance **2021**, 26, 140-147, doi:10.1016/j.jgar.2021.05.010.
3. Binert-Kusztal, Ż.; et al. Potential Use of Cefiderocol and Nanosilver in Wound Dressings to Control Multidrug-Resistant Gram-Negative Bacteria. Molecules **2025**, 30, doi:10.3390/molecules30153072.
4. Holzer-Geissler, J.C.J.; et al. The Impact of Prolonged Inflammation on Wound Healing. Biomedicines **2022**, 10, doi:10.3390/biomedicines10040856.
5. Hurlow, J.; Bowler, P.G. Acute and chronic wound infections: microbiological, immunological, clinical and therapeutic distinctions. Journal of wound care **2022**, 31, 436-445, doi:10.12968/jowc.2022.31.5.436.
6. Xu, X.; et al. Chitosan-based multifunctional hydrogel for sequential wound inflammation elimination, infection inhibition, and wound healing. International Journal of Biological Macromolecules **2023**, 235, 123847, doi:10.1016/j.ijbiomac.2023.123847.
7. Wang, Y.; et al. Inflammation-Responsive Drug-Loaded Hydrogels with Sequential Hemostasis, Antibacterial, and Anti-Inflammatory Behavior for Chronically Infected Diabetic Wound Treatment. ACS Applied Materials & Interfaces **2021**, 13, 33584-33599, doi:10.1021/acsami.1c09889.
8. Niculescu, A.-G.; et al. Zinc Alginate Hydrogel-Coated Wound Dressings: Fabrication, Characterization, and Evaluation of Anti-Infective and In Vivo Performance. Gels **2025**, 11, 427.
9. Alberts, A.; et al. Collagen-Based Wound Dressings: Innovations, Mechanisms, and Clinical Applications. Gels **2025**, 11, doi:10.3390/gels11040271.
10. Cristea, A.-G.; et al. Antimicrobial Smart Dressings for Combating Antibiotic Resistance in Wound Care. Pharmaceuticals **2025**, 18, doi:10.3390/ph18060825.
11. Niu, Y.; et al. Towards Intelligent Wound Care: Hydrogel-Based Wearable Monitoring and Therapeutic Platforms. Polymers **2025**, 17, doi:10.3390/polym17131881.
12. Kaya, S.; Derman, S. Properties of ideal wound dressing. Journal of Faculty of Pharmacy of Ankara University **2023**, 47, 1119-1131.
13. Nguyen, H.M.; et al. Biomedical materials for wound dressing: recent advances and applications. RSC Advances **2023**, 13, 5509-5528, doi:10.1039/D2RA07673J.
14. Orlińska, K.; et al. Wound healing – characteristics of the ideal dressing. Ann. Acad. Med. Siles. **2023**, 77, 197-203, doi:10.18794/aams/173203.
15. Sheokand, B.; et al. Natural polymers used in the dressing materials for wound healing: Past, present and future. Journal of polymer science **2023**, 61, 1389-1414.

16. Yoon, M.S.; et al. Dual-Drug Delivery Systems Using Hydrogel–Nanoparticle Composites: Recent Advances and Key Applications. Gels **2025**, 11, doi:10.3390/gels11070520.
17. Wang, W.; et al. Advances and challenges on hydrogels for wound dressing. Current Opinion in Biomedical Engineering **2023**, 26, 100443, doi:10.1016/j.cobme.2022.100443.
18. Wang, L.; et al. Multifunctional hydrogel as wound dressing for intelligent wound monitoring. Chemical Engineering Journal **2022**, 433, 134625, doi:10.1016/j.cej.2022.134625.
19. Shen, Z.; et al. Advances in Functional Hydrogel Wound Dressings: A Review. Polymers **2023**, 15, doi:10.3390/polym15092000.
20. Iqbal, Y.; et al. Alginate-Based hydrogels with inorganic Nanomaterials: A promising approach for wound healing and bone tissue regeneration. European Polymer Journal **2024**, 212, 113057, doi:10.1016/j.eurpolymj.2024.113057.
21. Liu, T.; et al. Nanomaterials and nanomaterials-based drug delivery to promote cutaneous wound healing. Advanced Drug Delivery Reviews **2023**, 193, 114670, doi:10.1016/j.addr.2022.114670.
22. Jin, S.-E.; et al. Hierarchical tetramodal-porous architecture of zinc oxide nanoparticles microfluidically synthesized via dual-step nanofabrication. Materials & Design **2022**, 215, 110486, doi:10.1016/j.matdes.2022.110486.
23. Li, Y.; et al. Recent Advances in Zinc Oxide Nanostructures with Antimicrobial Activities. International Journal of Molecular Sciences **2020**, 21, doi:10.3390/ijms21228836.
24. Pino, P.; et al. Antimicrobial Nano-Zinc Oxide Biocomposites for Wound Healing Applications: A Review. Pharmaceutics **2023**, 15, doi:10.3390/pharmaceutics15030970.
25. Batool, M.; et al. Adsorption, antimicrobial and wound healing activities of biosynthesised zinc oxide nanoparticles. Chemical Papers **2021**, 75, 893-907, doi:10.1007/s11696-020-01343-7.
26. Asif, N.; et al. Recent advances in the synthesis, characterization and biomedical applications of zinc oxide nanoparticles. Bioprocess and Biosystems Engineering **2023**, 46, 1377-1398, doi:10.1007/s00449-023-02886-1.
27. Popa, M.L.; et al. Traditional vs. Microfluidic Synthesis of ZnO Nanoparticles. International Journal of Molecular Sciences **2023**, 24, doi:10.3390/ijms24031875.
28. Kang, H.W.; et al. Continuous synthesis of zinc oxide nanoparticles in a microfluidic system for photovoltaic application. Nanoscale **2014**, 6, 2840-2846, doi:10.1039/C3NR06141H.
29. Alberts, A.; et al. Natural Products for Improving Soft Tissue Healing: Mechanisms, Innovations, and Clinical Potential. Pharmaceutics **2025**, 17, doi:10.3390/pharmaceutics17060758.
30. Kumarasamyraja, D.; et al. A review on medicinal plants with potential wound healing activity. Int J Pharm Pharm Sci **2012**, 2, 105-111.
31. Lammoglia-Ordiales, L.; et al. A randomised comparative trial on the use of a hydrogel with tepescohuite extract (Mimosa tenuiflora cortex extract-2G) in the treatment of venous leg ulcers. International Wound Journal **2012**, 9, 412-418, doi:10.1111/j.1742-481X.2011.00900.x.
32. Kokane, D.D.; et al. Evaluation of wound healing activity of root of Mimosa pudica. Journal of Ethnopharmacology **2009**, 124, 311-315, doi:10.1016/j.jep.2009.04.038.
33. Chircov, C.; et al. Synthesis of Magnetite Nanoparticles through a Lab-On-Chip Device. Materials **2021**, 14, doi:10.3390/ma14195906.
34. Bîrcă, A.C.; et al. A Microfluidic Approach for Synthesis of Silver Nanoparticles as a Potential Antimicrobial Agent in Alginate–Hyaluronic Acid-Based Wound Dressings. International Journal of Molecular Sciences **2023**, 24, doi:10.3390/ijms241411466.
35. Achehboune, M.; et al. Study on the effect of Er dopant on the structural properties of ZnO nanorods synthesized via hydrothermal method. 2019, 2019; p. 012020.
36. Khlifi, N.; et al. X-ray peaks profile analysis, optical and cathodoluminescence investigations of cobalt-doped ZnO nanoparticles. Journal of Luminescence **2022**, 245, 118770.

37. El-Desoky, M.; et al. Characterization and optical properties of annealed ZnO nanoparticles prepared by microwave irradiation. Frontiers in Scientific Research and Technology **2020**, 1, 1-7.
38. Aprilliza, M. Characterization and properties of sodium alginate from brown algae used as an ecofriendly superabsorbent. 2017, 2017; p. 012019.
39. Bîrcă, A.C.; et al. Infection-Free and Enhanced Wound Healing Potential of Alginate Gels Incorporating Silver and Tannylated Calcium Peroxide Nanoparticles. International Journal of Molecular Sciences **2024**, 25, doi:10.3390/ijms25105196.
40. Sabater i Serra, R.; et al. Bio-Nanocomposite Hydrogel Based on Zinc Alginate/Graphene Oxide: Morphology, Structural Conformation, Thermal Behavior/Degradation, and Dielectric Properties. Polymers **2020**, 12, doi:10.3390/polym12030702.
41. Wu, C.; et al. Porous Hydrogels for Immunomodulatory Applications. International Journal of Molecular Sciences **2024**, 25, doi:10.3390/ijms25105152.
42. Lai, C.M.; et al. Innovative hydrogel design: tailoring immunomodulation for optimal chronic wound recovery. Advanced Science **2025**, 12, 2412360.
43. Raha, S.; Ahmaruzzaman, M. ZnO nanostructured materials and their potential applications: progress, challenges and perspectives. Nanoscale advances **2022**, 4, 1868-1925.
44. Lordani, T.V.A.; et al. Therapeutic effects of medicinal plants on cutaneous wound healing in humans: a systematic review. Mediators of inflammation **2018**, 2018, 7354250.